Thermal response of structure and hydroxyl ion of phengite-2 M ₁: an in situ neutron diffraction and FTIR study

Article *in* European Journal of Mineralogy · May 2001

DOI: 10.1127/0935-1221/2001/0013-0545

CITATIONS
33

READS
34

3 authors:

Mainak Mookherjee
Florida State University
116 PUBLICATIONS **1,656** CITATIONS

SEE PROFILE

Simon Redfern
Nanyang Technological University
398 PUBLICATIONS **9,049** CITATIONS

SEE PROFILE

Ming Zhang
Institute of Materials, China Academy of Engineering Physics
132 PUBLICATIONS **3,227** CITATIONS

SEE PROFILE

Eur. J. Mineral.
2001, **13**, 545-555

This paper was presented at the EMPG VIII
meeting in Bergamo, Italy (April 2000)

Thermal response of structure and hydroxyl ion of phengite-2M_1: an *in situ* neutron diffraction and FTIR study

MAINAK MOOKHERJEE*, SIMON A.T. REDFERN AND MING ZHANG
Department of Earth Sciences, University of Cambridge, Cambridge CB2 3EQ, UK

Abstract: The thermal dependence of the structure of natural phengite-2M_1 with chemical formula $(K_{0.95}Na_{0.05})(Al_{0.76}Fe_{0.14}Mg_{0.10})_2(Si_{3.25}Al_{0.75})O_{10}(OH_{1.96}F_{0.04})$ has been studied by *in situ* neutron diffraction. The short-range correlated behaviour of the hydroxyl group was probed by FTIR spectroscopy while the long-range correlated hydroxyl structure was studied by neutron diffraction. Changes in long-range ordering of Si and Al on the tetrahedral sites were not observed from neutron diffraction. Structure refinement of the neutron diffraction data by the Rietveld method suggested that the apparent average hydroxyl bond length decreases on heating. The infrared data show a decrease in the stretching frequency of hydroxyl group, however. Possible explanations for these results are explored. It seems most likely that the apparent shortening of the hydroxyl bond length may be an artefact due to an increase in its vibrational amplitude. The anisotropic vibration of the hydroxyl bond as revealed by the anisotropic displacement parameters of H, increases so much that the average length (shown by the neutron refinement) appears to decrease at high temperatures while the local length of the bond, as indicated by FTIR results, increases.

Key-words: mica, phengite-2M_1, hydroxyl, neutron diffraction, FTIR, hydrogen bond.

Introduction

Micas are very common minerals occurring in a wide variety of geological environments. Dehydroxylation of micas (including the dehydroxylation of illitic clays) in sedimentary basins, in subduction environments, and in metamorphic rocks is a very important natural process. Addressing the problem of what actually controls the dehydroxylation behaviour of mica on an atomic scale is of crucial importance in understanding the global dynamics of water. Here we investigate the nature of the hydroxyl environment in phengite using diffraction and spectroscopic methods.

The structure of dioctahedral 2:1 mica consists of octahedral sheets sandwiched between tetrahedral $(Si,Al)O_4$ sheets, with two out of three octahedral sites occupied by divalent or trivalent metal cation (typically Al, Mg and Fe) (Fig. 1).

In the trioctahedral micas all octahedral sheets are occupied and the O(3)-H vector is perpendicular to the (001) plane resulting in maximum K^+-H^+ repulsion, whereas in dioctahedral mica the O(3)-H vector is inclined away from the (001) plane at an angle less than 90°. The angle between the O(3)-H vector and the (001) plane in such micas is observed to range from 1.3° to 23.1° (Giese, 1979). This leads to a strong interaction between the apical O atoms of tetrahedral sites and the O(3)-H group. Hydrogen bonds occur between H and the apical oxygen of tetrahedral sites as well as to the bridging oxygens of the tetrahedral sites making the O(3)-H bond within the hydroxyl group weaker (Farmer, 1974; Langer *et al*., 1981). The projection of the O(3)-H vector onto (001)

*e-mail: mm329@cam.ac.uk

DOI: 10.1127/0935-1221/2001/0013-0545

0935-1221/01/0013-0545 $ 2.75

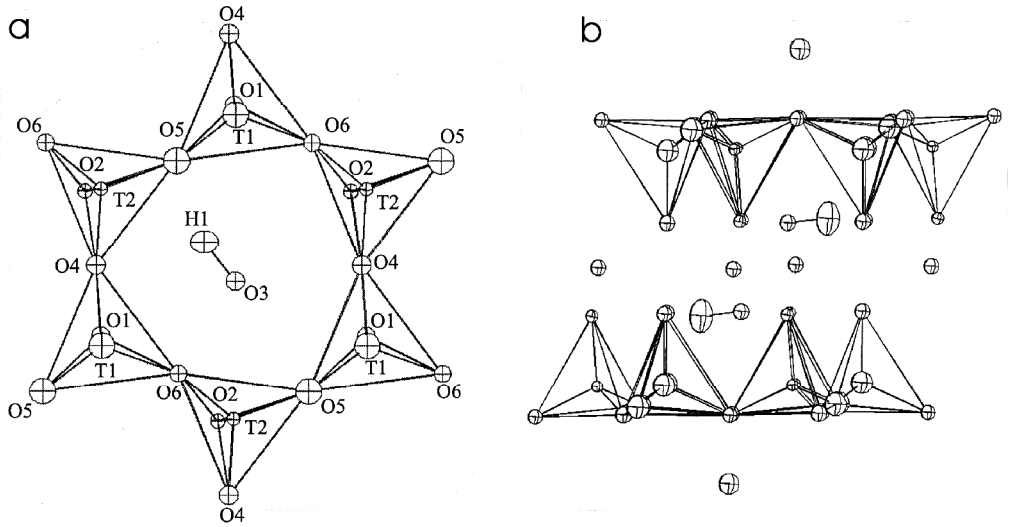

Fig. 1. a) A section of single ditrigonal ring formed by the TO_4 polyhedra perpendicular to the z^* direction (at 100°C). The interlayer potassium/sodium (not shown for clarity) sits at similar x,y position coordinate as that of the hydroxyl group (O(3)-H(1)) in the figure. The octahedral cations are omitted for clarity. Apical oxygen atoms, labelled O(1) and O(2) are part of T(1) and T(2) respectively and those labelled O(4), O(5) and O(6) are basal oxygen atoms. O(3) is the part of the hydroxyl group and is roughly at the center of the ring and at the same z coordinate as that of the O(1) and O(2) atoms. b) Two ditrigonal rings viewed perpendicular to (a). The major axis of the hydrogen thermal ellipsoid is at high angles to the hydroxyl bond. Structures are from our refinements of neutron data collected at 100°C.

makes an angle with the *b* axis, which ranges from –30° to 32° (Rouxhet, 1970).

A huge volume of work on the mica and mica-like minerals has been published and is reviewed to some extent in Bailey (1984). Early work on the dehydroxylation of mica was performed by Gaines & Vedder (1964). They demonstrated the loss of the hydroxyl group on heating, on the basis of the shift and disappearance of the O(3)-H peak in the IR spectrum. Most of the vibrational spectroscopic studies that have been carried out focus on the characterization of the environment of the hydroxyl group in terms of the nature of the cationic neighbours (Vedder, 1964; Wilkins & Ito, 1967; Farmer, 1974; Robert & Kodama, 1988), the influence of vacant octahedral site in the dioctahedral micas (Vedder & McDonald, 1963; Farmer, 1974; Langer *et al*., 1981), the influence of the tetrahedral layer through cationic substitution, *e.g*. Si-Al order disorder relations and layer distortions (Farmer & Russell, 1964; Farmer & Velde, 1973) and the effect of the orientation of the O(3)-H dipole (Serratosa & Bradley, 1958a and b) and the effect of the proton-interlayer cation repulsion (Kodama *et al*., 1974). Other studies include high temperature X-ray and neutron diffraction, investigating tetrahedral ordering (Pavese *et al*., 1999) and dehydroxylation mechanisms (Guggenheim *et al*., 1987).

Recent studies suggest that the stability of OH^- groups in micas is intimately linked to the site occupancies of metal cations in the octahedral sheet (Drits *et al*., 1995). The present work was initiated to study the relationship between the cation disorder (as a function of *T*) and dehydroxylation of micas.

The main aim of this study is to determine the temperature-dependence of the long-range order-disorder of the octahedral and tetrahedral sites and the behaviour of the proton using *in situ* high-temperature neutron powder diffraction. Infrared spectroscopy is sensitive to OH^- structure and short-range order, and it has been used as a complementary method to neutron diffraction.

Experimental procedure

The one phengite sample studied so far originated from Livadi mafic-ultramafic complexes, N.E. Greece. The Si^{4+} content of this phengite (Nance, 1976) varies from 3.20 to 3.50 per formu-

Table 1. Experimental and instrumental parameters pertaining to Rietveld refinements.

Instrumental	
Diffractometer	D2B (neutron powder diffractometer), ILL
Wavelength	1.5943 Å
Temperature	see Table 2
Refinement	
Space group	*C* 1 2/*c* 1
Z	2
Unit-cell refinements	whole pattern
Observations	2911
Refined parameters	
Structural	55
Profile	7
Background	10
Unit cell	4
Constraints	
Strict (equal U_{iso})	K1 = Na1, Al1 = Mg1 = Fe1, Si1 = Al2, Si2 = Al3
Strict (Σsite = 1)	K1 + Na1 = 1, Al1 + Fe1 + Mg1 = 1, Si1 + Al2 = 1, Si2 + Al3 = 1
Thermal Parameters	all atoms except hydrogen are isotropic
Agreement factors	see Table 2

la unit and indicates a metamorphic condition of about 250°C to 500°C at 0.5 GPa. The sample was characterised by electron probe microanalysis and the composition determined as $(K_{0.95}Na_{0.05})(Al_{0.76}Fe_{0.14}Mg_{0.10})_2(Si_{3.25}Al_{0.75})O_{10}(OH_{1.96}F_{0.04})$. The original sample was magnetically separated from the other impurities and then the phase was identified to be phengite-2M_1 polytype by powder X-ray diffraction, using a Philips X-ray diffractometer.

In situ high-temperature neutron-diffraction studies

This sample was studied using *in situ* high-temperature neutron powder-diffraction at the D2B diffractometer (λ = 1.5943 Å) at ILL, Grenoble, France. Approximately 3 cm^3 of phengite powder was loaded into a vanadium sample can within a vanadium furnace. Diffraction patterns were collected over a time span of four hours, a time interval which was chosen as the optimal compromise between being that the counting statistics on low-*d*-spacing peaks were small, while short enough that the data could be collected to high temperature without the risk of sample

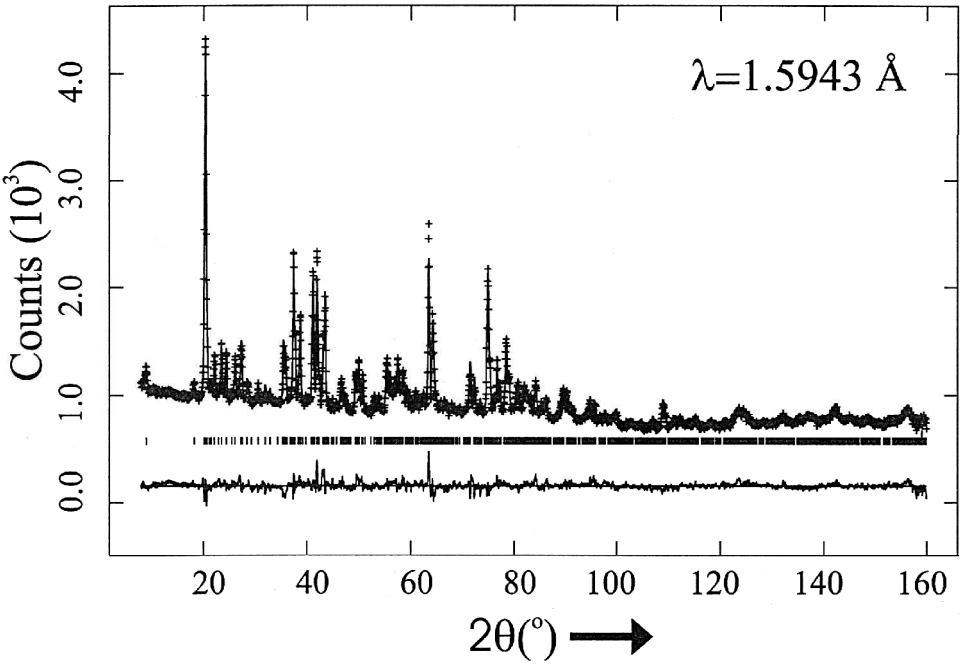

Fig. 2. Comparison of measured (crosses) and calculated (solid line) diffraction patterns (from Rietveld refinements of the crystal structure) of phengite (at 100°C). The lower curve shows the differences, and the tick marks show the peak positions.

Table 2. Room-temperature to high-temperature data of unit-cell parameter, fractional position coordinates, thermal displacement parameters and $R_p = \Sigma(|I_o-I_c| \cdot |I_o-I_b| / I_o) / \Sigma|I_o-I_b|$ and $wR_p = [\Sigma w((I_o-I_c)\cdot(I_o-I_b)/I_o)^2 / \Sigma(I_o-I_b)^2]^{1/2}$, where I and w are the intensities and weights of the profile points respectively, and I_b is the background contribution to the profile.

T(°C)	20	100	200	300	300	400	400	500	500	600	650	700
a(Å)	5.2173(1)	5.2196(2)	5.2230(2)	5.2276(2)	5.2279(2)	5.2321(2)	5.2324(2)	5.2360(2)	5.2356(2)	5.2356(2)	5.2412(2)	5.2328(2)
b(Å)	9.0493(2)	9.0550(3)	9.0618(3)	9.0701(3)	9.0745(3)	9.0784(3)	9.0787(3)	9.0862(3)	9.0893(3)	9.0893(3)	9.0983(3)	9.0948(3)
c(Å)	19.989(1)	20.010(1)	20.044(1)	20.083(1)	20.096(1)	20.125(1)	20.129(1)	20.169(1)	20.177(1)	20.177(1)	20.242(1)	20.207(1)
β (°)	95.734(4)	95.746(4)	95.738(4)	95.726(4)	95.727(4)	95.715(4)	95.718(4)	95.707(4)	95.707(4)	95.707(4)	95.690(5)	95.694(5)
Volume(Å)	938.99(7)	940.97(7)	943.90(7)	947.49(7)	948.62(7)	951.16(7)	951.42(7)	954.80(7)	955.43(7)	955.43(7)	960.47(8)	957.92(9)
K/Na												
y	0.087(2)	0.097(2)	0.095(2)	0.097(2)	0.098(2)	0.096(2)	0.098(2)	0.095(2)	0.093(2)	0.093(2)	0.090(3)	0.88(3)
U_{iso}*100(Å^2)	2.2(3)	2.4(3)	2.9(3)	3.8(3)	4.4(3)	4.8(4)	4.2(4)	5.2(4)	5.6(4)	5.6(4)	6.3(5)	6.4(5)
Al/Mg/Fe												
x	0.242(1)	0.236(2)	0.236(2)	0.235(2)	0.236(2)	0.233(2)	0.236(2)	0.234(2)	0.236(2)	0.236(2)	0.235(2)	0.234(2)
y	0.0834(7)	0.0814(8)	0.0811(8)	0.0808(9)	0.0807(8)	0.0795(9)	0.0822(9)	0.0797(9)	0.0804(8)	0.0805(8)	0.0807(9)	0.0799(9)
z	0.0009(7)	-0.0017(6)	-0.0014(6)	-0.0010(6)	-0.0012(6)	-0.0008(6)	-0.0012(6)	-0.0007(6)	-0.0009(6)	-0.0009(6)	-0.0009(7)	-0.0004(7)
U_{iso}*100(Å^2)	0.5(1)	1.1(2)	1.4(2)	1.6(2)	1.8(16)	1.7(2)	1.6(2)	1.8(2)	2.1(2)	2.1(2)	2.2(2)	2.2(2)
O1												
x	0.457(1)	0.455(1)	0.455(1)	0.458(1)	0.458(1)	0.458(1)	0.460(2)	0.458(2)	0.459(1)	0.459(1)	0.460(2)	0.461(2)
y	0.9398(7)	0.9425(8)	0.9420(8)	0.9430(8)	0.9434(8)	0.9438(8)	0.9435(9)	0.9439(9)	0.9447(8)	0.9447(8)	0.9443(9)	0.9446(9)
z	0.0513(5)	0.0522(5)	0.0523(5)	0.0521(5)	0.0532(5)	0.0524(5)	0.0520(5)	0.0521(5)	0.0533(5)	0.0534(5)	0.0531(6)	0.0541(6)
U_{iso}*100(Å^2)	1.3(2)	1.3(2)	1.5(2)	1.9(2)	2.2(2)	2.3(2)	2.1(2)	2.8(2)	2.9(2)	2.9(2)	3.2(3)	3.0(3)
O2												
x	0.394(1)	0.394(1)	0.394(1)	0.395(1)	0.394(1)	0.395(1)	0.395(1)	0.395(1)	0.394(1)	0.394(1)	0.394(1)	0.393(1)
y	0.2536(8)	0.2559(9)	0.2572(9)	0.2566(9)	0.2555(9)	0.2571(9)	0.2574(9)	0.2571(9)	0.2560(9)	0.2560(9)	0.2571(9)	0.2565(10)
z	0.0521(4)	0.0542(4)	0.0541(4)	0.0545(4)	0.0548(4)	0.0543(4)	0.0542(4)	0.0544(4)	0.0545(4)	0.0545(4)	0.0540(4)	0.0539(4)
U_{iso}*100(Å^2)	1.1(1)	0.8(1)	0.9(1)	1.3(2)	1.6(2)	1.5(2)	1.4(2)	1.6(2)	1.8(2)	1.9(2)	2.0(2)	2.0(2)

T(°C)	20	100	200	300	300	400	400	500	500	600	650	700
O3												
x	0.454(1)	0.459(1)	0.462(1)	0.460(1)	0.459(1)	0.459(1)	0.457(1)	0.460(1)	0.459(1)	0.459(1)	0.459(2)	0.457(2)
y	0.5620(6)	0.5610(7)	0.5605(7)	0.5609(8)	0.5607(8)	0.5614(8)	0.5608(8)	0.5617(8)	0.5609(9)	0.5608(9)	0.5610(9)	0.5609(9)
z	0.0520(5)	0.0509(5)	0.0507(5)	0.0511(5)	0.0507(5)	0.0511(5)	0.0501(5)	0.0510(5)	0.0505(5)	0.0505(5)	0.0499(6)	0.0494(6)
U_{iso}*100(Å^2)	1.2(2)	1.4(2)	1.5(2)	2.2(2)	2.6(2)	2.5(2)	1.8(2)	2.6(2)	2.9(2)	2.9(2)	3.1(2)	2.7(2)
H1												
x	0.350(3)	0.342(3)	0.339(3)	0.338(3)	0.343(3)	0.339(4)	0.338(4)	0.342(4)	0.344(4)	0.344(4)	0.341(4)	0.347(5)
y	0.656(1)	0.647(2)	0.647(2)	0.646(2)	0.643(2)	0.644(2)	0.644(2)	0.645(2)	0.641(2)	0.641(2)	0.642(2)	0.642(2)
z	0.052(1)	0.056(1)	0.057(1)	0.057(1)	0.058(1)	0.057(1)	0.059(1)	0.059(1)	0.059(1)	0.059(1)	0.057(2)	0.057(2)
U_{11}*100(Å^2)	6.1(1)	8.1(1)	8.3(1)	10.4(1)	10.9(1)	12.4(2)	14.9(2)	14.1(2)	13.2(2)	13.3(2)	17.7(2)	20.0(3)
U_{22}*100(Å^2)	4.7(1)	4.7(1)	6.0(1)	4.3(1)	5.2(1)	5.2(1)	5.8(1)	4.8(1)	4.4(1)	4.4(1)	3.7(1)	2.8(1)
U_{33}*100(Å^2)	4.3(2)	8.6(2)	8.4(2)	7.1(2)	10.0(3)	11.5(3)	13.6(3)	14.5(3)	17.8(4)	18.0(4)	22.0(4)	24.0(5)
U_{12}*100(Å^2)	4.8(1)	4.7(1)	5.8(1)	5.7(1)	6.0(1)	6.8(1)	7.7(1)	7.0(1)	5.9(1)	6.0(1)	6.9(1)	6.4(1)
U_{13}*100(Å^2)	5.3(1)	4.4(1)	4.6(1)	2.7(1)	1.1(1)	5.8(2)	8.3(2)	6.2(2)	3.8(2)	3.7(2)	10.3(1)	9.9(3)
U_{23}*100(Å^2)	3.5(1)	0.3(1)	-0.2(1)	0.1(1)	0.2(1)	1.6(1)	0.8(1)	1.7(1)	0.4(1)	0.2(1)	1.9(1)	1.7(1)
T1												
x	0.462(1)	0.459(2)	0.458(2)	0.457(2)	0.457(2)	0.456(2)	0.455(2)	0.456(2)	0.455(2)	0.455(2)	0.455(2)	0.456(2)
y	0.925(1)	0.921(1)	0.920(2)	0.922(1)	0.924(1)	0.921(1)	0.922(2)	0.920(1)	0.922(1)	0.922(1)	0.921(2)	0.922(2)
z	0.1350(7)	0.1347(7)	0.1335(7)	0.1327(7)	0.1328(7)	0.1332(7)	0.1321(7)	0.1330(7)	0.1317(7)	0.1316(7)	0.1320(7)	0.1317(8)
U_{iso}*100(Å^2)	1.5(2)	2.7(3)	3.2(3)	2.9(3)	3.4(3)	3.2(3)	3.2(3)	3.4(3)	3.6(3)	3.6(3)	3.6(3)	4.2(3)
T2												
x	0.452(1)	0.453(1)	0.454(1)	0.453(1)	0.452(1)	0.451(1)	0.452(1)	0.451(1)	0.450(1)	0.450(1)	0.451(1)	0.449(1)
y	0.260(1)	0.261(1)	0.261(1)	0.262(1)	0.263(1)	0.263(1)	0.264(1)	0.264(1)	0.264(1)	0.264(1)	0.265(1)	0.264(1)
z	0.1377(6)	0.1362(6)	0.1363(6)	0.1362(5)	0.1355(5)	0.1346(5)	0.1353(6)	0.1342(5)	0.1340(5)	0.1339(5)	0.1335(6)	0.1324(6)
U_{iso}*100(Å^2)	0.6(2)	0.7(2)	0.7(2)	0.5(2)	0.8(2)	0.8(2)	0.9(2)	0 .8(2)	1.2(2)	1.2(2)	1.4 (2)	1. 3(2)

T(°C)	20	100	200	300	300	400	400	500	500	600	650	700
O4												
x	0.429(1)	0.436(1)	0.437(1)	0.439(1)	0.442(1)	0.441(1)	0.439(1)	0.443(1)	0.446(1)	0.446(1)	0.450(1)	0.450(1)
y	0.0955(7)	0.0957(7)	0.0960(7)	0.0960(8)	0.0958(8)	0.0964(8)	0.0968(9)	0.0969(8)	0.0969(8)	0.0969(8)	0.0979(9)	0.0983(9)
z	0.1688(5)	0.1687(4)	0.1682(4)	0.1677(4)	0.1686(4)	0.1678(4)	0.1676(5)	0.1675(4)	0.1686(4)	0.1687(4)	0.1687(5)	0.1692(5)
U_{iso}*100(Å^2)	1.9(2)	1.5(2)	1.7(2)	2.1(2)	2.5(2)	2.6(2)	2.6(2)	3.0(2)	3.1(2)	3.1(2)	3.7(2)	3.6(2)
O5												
x	0.231(1)	0.237(2)	0.231(2)	0.230(2)	0.231(1)	0.227(1)	0.226(2)	0.225(1)	0.226(1)	0.226(1)	0.224(2)	0.226(2)
y	0.8205(7)	0.8209(8)	0.8227(8)	0.8252(8)	0.8243(7)	0.8269(7)	0.8264(8)	0.8283(7)	0.8268(7)	0.8268(7)	0.8282(8)	0.8266(8)
z	0.1591(7)	0.1594(6)	0.1593(6)	0.1588(6)	0.1579(6)	0.1582(6)	0.1583(6)	0.1581(6)	0.1577(6)	0.1577(6)	0.1578(6)	0.1574(6)
U_{iso}*100(Å^2)	2.8(2)	2.8(2)	3.0(2)	3.2(2)	3.3(2)	3.1(2)	3.1(2)	3.2(2)	3.4(2)	3.4(2)	3.7 (2)	3. 6(2)
O6												
x	0.248(1)	0.246(1)	0.246(1)	0.246(1)	0.243(1)	0.243(1)	0.243(1)	0.242(1)	0.241(1)	0.241(1)	0.239(2)	0.239(2)
y	0.3644(6)	0.3601(6)	0.3587(6)	0.3578(6)	0.3574(6)	0.3566(6)	0.3567(7)	0.3547(6)	0.3548(6)	0.3548(6)	0.3537(7)	0.3549(7)
z	0.1693(6)	0.1704(5)	0.1703(5)	0.1714(5)	0.1711(5)	0.1718(5)	0.1708(5)	0.1713(5)	0.1710(5)	0.1710(5)	0.1700(9)	0.1704(6)
U_{iso}*100(Å^2)	1.6(2)	1.2(2)	1.3(2)	2.0(2)	2.0(2)	2.3(2)	2.1(2)	2.5(2)	2.8(2)	2.8(2)	3.3 (2)	3. 4(2)
WR_p	4.47	4.37	4.24	4.1	4.01	3.94	4.09	3.81	3.72	3.71	3.64	3.65
R_p	3.31	3.31	3.19	3.1	3.05	2.99	3.12	2.92	2.86	2.83	2.79	2.83

break down. Data were obtained from 293 to 973 K and on cooling at 773 K, 673 K, and 573 K under vacuum for four hours each (Table 1). Using the information we obtained from X-ray diffraction, we were able to refine these patterns by Rietveld analysis (Rietveld, 1969) using the GSAS software package (Larson & Von Dreele, 1986) (Fig. 2) and a 2M_1 mica structural model (Guggenheim *et al.*, 1987). We tested for the presence of phengite-3*T*, using the structural model of Pavese *et al.* (1999), which was incorporated as a second phase within the refinement. Peaks attributable solely to phengite-3*T* (*i.e.* ones that do not overlap with those of 2M_1) are absent from our patterns. Most noticeably, there is no evidence of intensity at the position of the (1 0 5) and (1 0 7) peaks of the 3*T* structure between 25° and 30° 2θ. The peak shape profile was a pseudo-Voigt function and the background was modelled with a ten-term shifted-Chebyshev function. The preferred orientations have been taken into account using the Dollase (1986) model. A constrained refinement scheme has been adopted because of the structural complexity of the mineral. Accordingly the following procedure was adopted:

i) the thermal factors for all atoms except H were considered as isotropic;

ii) cation ordering was constrained to the original room-temperature value since no significant change could be observed and no regular pattern was observed among the Al and Si occupancies across the tetrahedral sites;

iii) the fractional co-ordinates of the atoms were refined unconstrained.

All data were refined until convergence was achieved. The *R*-factors corresponding to the Bragg contribution to the diffraction pattern (*i.e.* not including the contributions from background) are listed in Table 2, where this value represents

$R_p = \Sigma(|I_o - I_c| \cdot |I_o - I_b| / I_o) / \Sigma|I_o - I_b|$.

Infrared spectroscopy studies

Silicon wafers have been successfully used as infrared windows in other studies of minerals at high *T* (Bray, 1999; Bray & Redfern, 2000). A small amount (approximately 2.5 mg) of the powdered sample was applied to the wafer with a spatula, in order to obtain a usable area 13 mm in diameter. For high-temperature *in situ* infrared measurements, the sample was positioned within a cylindrical platinum-wound furnace with a recycle-water-cooling system. The cooling system was used to avoid the outside of the furnace to become too hot. Two thermocouples were equipped in the furnace. The heating and cooling of the furnace was controlled by using a Pt/PtRh thermocouple located close to the heating platinum wires in the furnace and an Eurothermal 815 temperature controller, which allowed a temperature stability of less than ± 1 K. The temperature of specimen was measured by using a NiCr/NiAl thermocouple which was pressed against the sample and coupled with a Comark microprocessor thermometer. The thermocouple was calibrated against the α-β phase transition in quartz and cristobalite. The heating rate was 15°C min^{-1}. The spectra were collected under vacuum with a Brucker 113v FTIR spectrometer. A liquid-nitrogen-cooled mercury-cadmium-telluride detector coupled to a KBr beam splitter was used to record near infrared region (NIR) spectra. The spectral resolution was 4 cm^{-1}. A total of 150 scans was accumulated for each NIR spectrum. All spectra were recorded as absorbance α, with $\alpha = -\log_{10}(I_{\text{sample}}/I_{\text{reference}})$, where *I* is the single-beam transmission intensity. Spectra were recorded both in runs lowering and increasing temperature and the spectra obtained from heating and cooling are similar. Spectra are shown in Fig. 3.

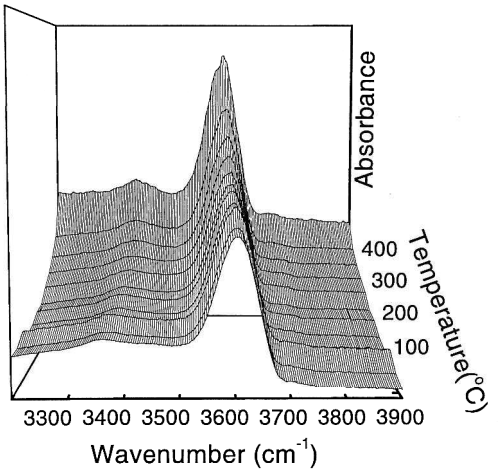

Fig. 3. Three-dimensional plot of the infrared spectra corresponding to hydroxyl streching region, with varying temperature.

Results and discussion

Lattice expansions

The neutron diffraction pattern gives the cell-parameter evolution as a function of temperature.

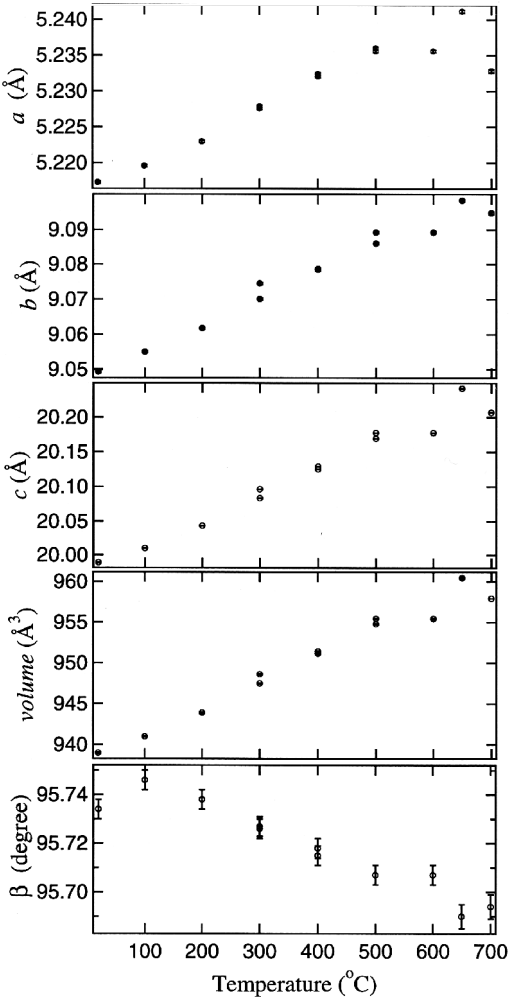

Fig. 4. Variation of a, b, c, volume and β with temperature. The two data points for each of the lattice parameters, at 300, 400 and 500°C corresponds to the heating and cooling respectively. Note: the error bars corresponding to a, b, c, and volume are smaller than the size of data points.

In Fig. 4 the cell parameters are shown as a function of temperature and these data are tabulated in Table 2. The linear thermal expansions of the cell parameters are anisotropic (characteristic of most sheet silicates) with coefficients $\alpha_a = 4.29$, $\alpha_b = 7.38$, and $\alpha_c = 16.61 \cdot 10^{-6}$ K^{-1}. We find that the cell edges show an apparent decrease at the highest temperature of our experiment. Guggenheim *et al.*, (1987) and Comodi & Zanazzi (2000) on the other hand found that the apparent thermal expansion of mica increases anomalously upon high-temperature dehydroxylation. Their samples were heated under atmospheric conditions (in air) or in a sealed evacuated tubes, and it is possible that dehydroxylation was accompanied by the oxidation of the transition metals in the structure. Our sample was heated in a vanadium can. Since vanadium acts as a highly efficient oxygen-getter, it is extremely unlikely that our sample was at all oxidised on heating. In fact, if anything, it is likely to have been reduced. This may account for the reduction of the cell edges seen in our sample at the highest temperatures.

The b cell parameter does not show the large increase seen at high temperature by Comodi & Zanazzi (2000). This gives support to our view that our sample has not oxidised or undergone any dehydroxylation. A view further confirmed by the refined occupancy of the H site, which is close to unity for all temperatures.

Tetrahedral site occupancies

Refinements of T1 and T2 site occupancies with respect to Al and Si contents show no regular pattern of change in ordering and remain constant within error across the entire temperature range. This is in accordance with the <T1-O> and <T2-O> bond lengths which show no variation within the average error of 0.15 Å. Table 3 shows that there is a decrease in the T1-O1, T1-O4, and T1-O5 bond lengths but an increase in the T1-O6 bond length from room temperature to high temperature. These opposing effects compensate each other. A similar phenomenon is observed at the T2 site with T2-O4, T2-O5, and T2-O6 all increasing on heating whereas T2-O2 decreases substantially to counterbalance the effect produced by them.

Table 3. Variation of tetrahedral bond lengths (in Å) with temperature.

T/K	293	973
T1-O1	1.676(16)	1.588(17)
T1-O4	1.705(12)	1.775(17)
T1-O5	1.641(11)	1.614(13)
T1-O6	1.668(12)	1.715(14)
<T1-O>	1.672(6)	1.673(8)
T2-O2	1.709(16)	1.584(15)
T2-O4	1.620(12)	1.684(13)
T2-O5	1.574(10)	1.591(12)
T2-O6	1.601(11)	1.628(12)
<T2-O>	1.626(6)	1.622(7)

These results do not indicate any significant changes in the degree of Al/Si order on the T-sites of our sample, at least over the time scale of our experiment (approximately four hours at each temperature). Pavese *et al.* (1999), however, suggests that such re-ordering may occur, on the basis of experiments carried out at HRPD (Rutherford Appleton Laboratory) over time scales at higher temperature.

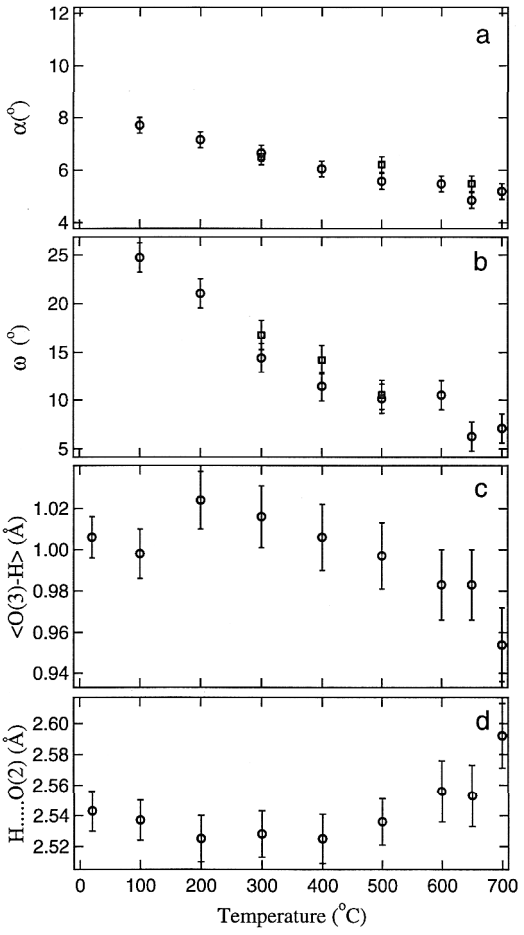

Fig. 5. **a**.Variation of ditrigonal distortion, with temperature. With no distortion, O(4)–O(5)–O(6) = 120°C and hence α is zero. The open circle represents the data collected while heating whereas the open square represents the data collected while cooling. **b**. Variation of ω, the angle that O(3)-H vector makes with the (001) plane, with temperature. The open circle represents the data collected while heating whereas the open squre represents the data collected while cooling. **c**. Variation of the average O(3)-H bond length with temperature as obtained from the neutron diffraction data. **d**. Variation of the H…O(2) (possible) hydrogen bond length with temperature.

Interlayer cations

The interlayer cation (K, Na)-O bond lengths show greater variation with temperature than do others. We find expansivities for individual bonds $\alpha_{<K\text{-}O4>}$, $\alpha_{<K\text{-}O4'>}$, $\alpha_{<K\text{-}O5>}$, $\alpha_{<K\text{-}O5'>}$, $\alpha_{<K\text{-}O6>}$ and $\alpha_{<K\text{-}O6'>}$ of $-2.58 \cdot 10^{-5}$, $4.56 \cdot 10^{-5}$, $-2.95 \cdot 10^{-5}$, $9.0 \cdot 10^{-5}$, $1.33 \cdot 10^{-5}$ and $0.572 \cdot 10^{-5}$ K^{-1} respectively. The interlayer cation forms three shorter bonds and three longer outer bonds forming ditrigonal rings. As the temperature increases these expansivities mean that the ditrigonal distortion of the ring decreases. This distortion is traditionally described by a parameter

$$\alpha = \left(120° - \overline{\langle O(4) - O(5) - (06)\rangle}\right)/2$$

where

$$\overline{\langle O(4) - O(5) - (06)\rangle}$$

is the average of the angles formed by trios of adjacent basal oxygens, and its temperature dependence is shown in Fig. 5a. The reduction in α with temperature results from rotations of the TO_4 tetrahedra on heating.

Octahedral cations

The M-O(3) bond length remains constant within error on heating. We might anticipate that dehydroxylation would result in shortening of M-O(3) bond, due to under-bonding of O(3). The fact that the M-O(3) bond remains the same length further confirms the lack of dehydroxylation found in the temperature range and conditions of this study, and also suggests that the occupancy of the M-site does not change on heating, at least on the time scale of our experiments.

Hydroxyl behaviour

Neutron diffraction is highly sensitive to hydrogen, due to the large scattering length of H. The large incoherent cross section of H typically generates a large background on the neutron diffraction patterns of hydrogenous materials. The H-content of mica is however, sufficiently small to allow good diffraction data to be obtained. We were therefore able to refine the hydrogen position as a function of temperature. The position of the hydrogen atom was refined unconstrained at all temperatures, using anisotropic displacement parameters and an occupancy factor of 1.0. Refinements allowing the H-occupancy to vary showed that it remains unity at all temperatures of our study, to within one standard deviation. The

O(3)-H bond length at 100°C is 0.998(2) Å and the bond is inclined at 24.7° (ω) to the (001) plane and is directed towards the *trans* M_1 vacant site. The projection of the O(3)-H bond on the (001) plane makes an angle $\psi = 44.32°$ with the [010] direction. The angle ω decreases to around 5° at the highest temperature of our study (Fig. 5b). The O(3)-H bond length, however, decreases with temperature (Fig. 5c). From infrared (IR) studies, Vedder & McDonald (1963) suggested that O(3)-H vector lies in a plane perpendicular to (001) and the trace of this plane on the (001) plane makes an angle of 32° with the *b* axis, with the vector itself inclined at 16° to (001) plane. However, Giese (1979) suggested that the angle made by the O(3)-H vector with the (001) plane varies between 1.3° to 23.1°. Our results indicate that the vector is at the upper end of this range.

One possible explanation of the net shortening of the O(3)-H bond that we observe on heating could be invoked by considering the possible interaction between the proton and the two apical oxygen that lie at the same *z* coordinate as well as the nearest bridging oxygen within the ring (Saksena, 1964). The (O...O), (H...O) distances and (O(3)-H...O) bond angles of the present study indicate a possibility of very weak hydrogen bonding (Libowitzky, 1999), in particular between H and O(2) (Fig. 5d). This pair are separated by around 2.54 Å, with the O(3)-H…O(2) angle lying at around 150°. This large *d*(H...O) distance indicates a potential hydrogen bond, albeit very weak. Furthermore, the relatively low values of (O(3)-H...O) angles are characteristic of non-linear and possibly trifurcated hydrogen bonds, as observed over a large number of organic crystals studied by neutron diffraction (Ceccarelli *et al*., 1981). At lower temperatures, therefore, the O(3)-H bond might be regarded as being stretched due to the weak hydrogen bonding to O(2). However, with increasing temperature any very weak hydrogen bonding to distant oxygen would presumably get weaker and the proton would retract back towards the O(3) atom, shortening the O(3)-H bond, as we observe.

Further information about the hydrogen environment comes from our infrared data, which show shifts of the hydroxyl stretching peak position (at around 3600 cm^{-1}) with temperature, as shown in Fig. 3. Chemical shifts of this peak have previously been correlated with variations in octahedral cation occupancy at the sites adjacent to the hydroxyl. For example, Besson *et al*. (1987) studied octahedral cation distribution in micas and found different degrees of cation segregation. The hydroxyl stretching frequency beween 3500 cm^{-1} and 3650 cm^{-1} is correlated with the mass and valency of the octahedral cation pair (Robert & Kodama, 1988; Besson & Drits, 1997), bands due to different cation pairs often overlap, and this seems to be the situation in our case. It would be difficult to infer anything about the octahedral occupancies from the peak at 3602 cm^{-1} in our sample.

In addition, we find a broad absorption at 3400 cm^{-1}, which is also assumed due to the O-H stretching mode. Substitution of Al^{3+} for Si^{4+} in the tetrahedral site creates a negative charge on the basal oxygen. According to Van der Maal & Beutelspacher (1976), water molecules, which form strong hydrogen bonds, associated to the negative charge on the basal oxygen, will absorb near 3400 cm^{-1}, and we assign this band to water at the basal surface.

The position of the main infrared absorption peaks changes from 3602 cm^{-1} at room temperature to 3594 cm^{-1} at 440°C (Fig. 6). It is known that if there is a secondary attachment, *e.g*. a hydrogen bond to the adjacent oxygen, the frequency should be lowered, and one might ascribe this change to a change in the bonding at the hydrogen atom. In this case, these infrared data would not support our model (above) for the decrease of the O(3)-H bond length with temperature, suggested by the neutron diffraction results. We would expect the frequency of absorption to increase if the hydrogen bonds to the apical oxygens becomes weaker. On the other hand, the temperature range of our infrared results is considerably less than that of the neutron data, and the frequency may begin to increase at higher temperatures. Furthermore, this small change in frequency (only 8 cm^{-1}) might also simply result

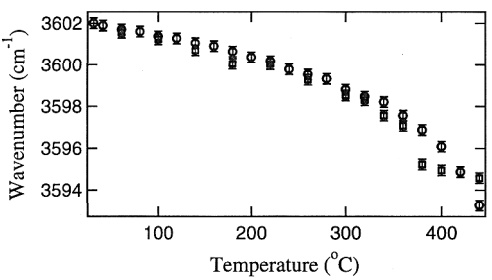

Fig. 6. Variation of the hydroxyl stretching frequency with temperature. The open circle represents the data collected while heating whereas the open square represents the data collected while cooling.

from coupling to the small changes in structure of the aluminosilicate sheet framework that we have already noted, since the dynamical matrix of the crystal will be altered by these structural readjustments. An exhaustive answer to the origin of this peak shift would require a more complete assessment of the dynamics of the mica structure, and in particular of the hydroxyl behaviour as a function of temperature or structural distortion, which is beyond the scope of this particular study.

We note that the possible discrepancy between the results from infrared spectroscopy and from diffraction of our study is quite comparable to that observed in case of the proton position and dynamics in hemimorphite (Libowitzky *et al.*, 1997). They explained this mismatch by considering the dynamic behaviour of proton position, which was evident in their diffraction results from elongated, smeared anisotropic displacement ellipsoids.

We also note that the displacement parameter of the hydrogen atom increases significantly on heating, which we interpret as increased librational amplitude of the O(3)-H group. The anisotropic displacement is principally perpendicular to the bond, which is quite comparable to the result of neutron and X-ray diffraction work on the hydroxyl ions in hydrogarnet (Lager *et al.*, 1987). The temperature variation of the equivalent isotropic temperature factor (U_{iso}) for the H-atom is shown in Fig. 7. This increases three-fold over the temperature range of our study. In light of this, it seems quite possible that the apparent shortening of the O(3)-H bond length may be an artefact and that vibration of this bond increases so much on heating (Fig. 8) that the average length (shown by the neutron refinement) appears to decrease while the length of the bond actually increases.

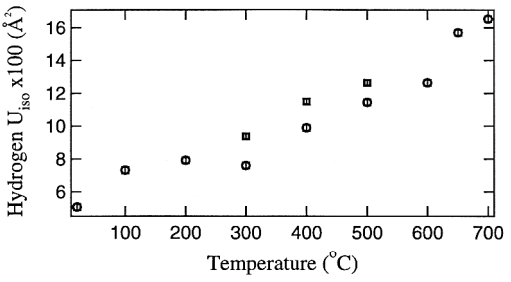

Fig. 7. Variation of the equivalent U_{iso} of the hydrogen atom with temperature, from the refined anisotropic temperature factor. The open circle represents the data collected while heating whereas the open square represents the data collected while cooling.

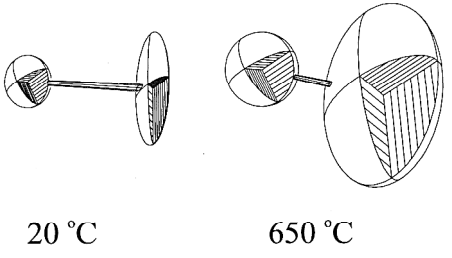

Fig. 8. ORTEP generated figures for the thermal ellipsoid of OH^- group at 20°C and 650°C. The ellipsoid shows the 50 % probability distribution of the scattering density, given by the anisotropic displacement parameters, and demonstrates the increase in librational amplitude of the hydroxyl group with the temperature.

Conclusions

On the basis of the results from the *in situ* high-temperature neutron powder diffraction (293-973 K) and FTIR spectroscopic experiments (293-713 K) on phengite-2M_1, the following conclusions are drawn:

1) Tetrahedral Al/Si atoms are partially disordered, both at room and high temperature, as suggested by refinements of the high-temperature data. We do not find that Al orders onto T1 in the time scale of our experiments. These results are in agreement with the analysis of tetrahedral bond distances.

2) The average hydroxyl group bond length decreases with increasing temperature. This could be explained by the formation of a hydrogen bond to O(2), the next nearest oxygen to H. This hydrogen bond becomes weaker on heating and the H…O(2) length increases. The H atom then moves back towards the hydroxyl oxygen O(3), with a decrease in the O(3)-H bond length. The infrared data, however, show that the hydroxyl stretching frequencies decrease with increasing temperature. This possibly contradicts these explanations of the neutron results, if we assume that this frequency decrease is due to the differences in hydrogen bonds to O(2). Such an assumption remains to be thoroughly tested. Thirdly, we note that the apparent shortening of the O(3)-H bond length could be an artefact due to an increase in the anisotropic vibration of the O(3)-H bond (Table 2), which increases so much that the average length (as shown by the neutron refinement) appears to decrease while the length of the bond actually increases, as indicated by FTIR results.

3) The expansion of the potassium site is anisotropic, and can be explained in terms of the thermal response of the ditrigonal rings on heating, as they become less distorted.

Acknowledgements: The authors thank H. Bray and A. Hewat for experimental assistance at Grenoble. Manuscripts were greatly improved through the constructive criticism of J.R. Smyth and one anonymous referee. MM acknowledges the financial support of the Cambridge Commonwealth Trust and the ORS.

References

Bailey, S.W. (1984): Classification and structures of the micas. *in* " Micas", S.W. Bailey, ed. Mineralogical Society of America. *Rev. Mineral.*, **13**, 584 p.

Besson, G. & Drits, V.A. (1997): Refined relationships between chemical compositions of dioctahedral fine grained micaceous minerals and their infrared spectra within the OH stretching region. Part II-The main factors affecting OH^- vibrations and quantitative analysis. *Clays Clay Minerals*, **45**, 70-183.

Besson, G., Drits, V.A., Daynyak, L.G., Smoliar, B.B. (1987): Analysis of cation distribution in the dioctahedral micaceous minerals on the basis of IR spectroscopy data. *Clay Minerals*, **22**, 465-475.

Bray, H.J. (1999): Kinetics of high-temperature transformations of clay minerals. PhD thesis, Univ. Cambridge, UK.

Bray, H.J. & Redfern, S.A.T. (2000): Influence of the counterion species on the dehydroxylation of Ca^{2+}-, Mg^{2+}, Na^+- and K^+-exchanged Wyoming montmorillonite. *Min. Mag.*, **64**, 337-346.

Ceccarelli, C., Jeffrey, G.A., Taylor, R. (1981): A survey of O-H...O hydrogen bond geometries determined by neutron diffraction. *J. Mol. Struct.*,**70**, 255-271.

Comodi, P. & Zanazzi, P.F. (2000): Structural thermal behaviour of paragonite and its dehydroxylate: a high-temperature single crystal study. *Phys. Chem. Minerals*, **27**, 377-385.

Dollase, W.A. (1986): Correction of intensities for preferred orientation in powder diffractometry: application of March model. *J. Appl. Cryst.*, **19**, 267-272.

Drits, V.A., Besson, G., Muller, F. (1995): An improved model for structural transformations of heat-treated aluminous dioctahedral 2:1 layer silicates. *Clays Clay Minerals*, **43**, 718-731.

Farmer, V.C. (1974): The layer silicates. *In*: Farmer, V.C, ed. "The infrared spectra of minerals". London: The Mineral. Soc., 331-364.

Farmer, V.C. & Russell, J.D. (1964): The infra-red spectra of layer silicates. *Spectrochim. Acta*, **20**, 1149-1173.

Farmer, V.C. & Velde, B. (1973): Effects of structural order and disorder on the infrared spectra of brittle micas. *Min. Mag.*, **39**, 282-288.

Gaines, G.L. & Vedder, W. (1964): Dehydroxylation of muscovite. *Nature*, **201**, 495.

Giese, R.F. (1979): Hydroxyl orientation in 2:1 phyllosilicates. *Clays Clay Minerals*, **35**, 170-171.

Guggenheim, S., Chang, Y.-H., Koster Van Groos, A.F. (1987): Muscovite dehydroxylation: High-temperature studies. *Am. Mineral.*, **72**, 537-550.

Kodama, H., Ross, G.J., Iiyama, J.T., Robert, J.-L. (1974): Effect of layer charge location on potassium exchange and hydration of micas. *Am. Mineral.*, **59**, 491-495.

Lager, G.A., Armbruster,T., Faber, J. (1987): Neutron and X-ray diffraction of hydrogarnet $Ca_3Al_2(O_4H_4)_3$. *Am. Mineral.*, **72**, 756-765.

Langer, K., Chatterjee, N.D., Abraham, K. (1981): Infrared studies of some synthetic and natural $2m_1$ dioctahedral micas. *N. Jb. Min. Abh.*, **142**, 91-110.

Larson, A.C. & Von Dreele, R.B. (1986): GSAS: General Software Analysis System manual. Los Alamos National Laboratory report. LAUR: 86-87

Libowitzky, E. (1999): Correlation of O-H stretching frequencies and O-H...O hydrogen bond lengths in Minerals. *Monatshefte für Chemie*, **130**, 1047-1059.

Libowitzky, E., Kohler, T., Armbruster, T., Rossman, G. (1997): Proton disorder in dehydrated hemimorphite - IR spectroscopy and X-ray structure refinement at low and ambient temperatures. *Eur. J. Mineral.*, **9**, 803-810.

Nance, R.D. (1976): The Livadi mafic-ultramafic complex and its metamorphic basement, N.E. Greece. PhD thesis, Univ. Cambridge, UK.

Pavese, A., Ferraris, G., Pischedda, V., Ibberson, R. (1999): Tetrahedral order in phengite $2M_1$ upon heating, from powder neutron diffraction, and thermodynamic consequences. *Eur. J. Mineral.*, **11**, 309-320.

Rietveld, H. M. (1969): A profile refinement method for nuclear and magnetic structures. *J. Appl. Cryst.*, **2**, 65-71.

Robert, J.-L. & Kodama, H. (1988): Generalization of the correlation between hydroxyl-stretching wave numbers and composition of micas in the system K_2O-MgO-Al_2O_3-SiO_2-H_2O: A single model for trioctahedral and dioctahedral micas. *Amer. J. Sci.*, **288**, 196-212.

Rouxhet, P.G. (1970): Hydroxyl stretching bands in micas: a quantitative interpretation. *Clay Minerals*, **8**, 75-388.

Saksena, B.D. (1964): Infrared hydroxyl frequencies of muscovite, phlogopite and biotite micas in relation to their structures. *Trans. Faraday Soc. (London)*, **60**, 1715-1725.

Serratosa, J.M. & Bradley, W. F. (1958a): Infrared absorption of OH^- bonds in micas. *Nature*, **181**, 111.

— , — (1958b): Determination of the orientation of OH-bond axes in layer silicates by infrared absorption. *J. Phys. Chem.*, **62**, 1164-1167.

Van der Maal, H.M. & Beutelspacher, H. (1976): Atlas of infrared spectroscopy of clay minerals and their admixtures. Elsevier, Amsterdam, 104 p.

Vedder, W. (1964): Correlation between infrared spectrum and chemical composition of mica. *Am. Mineral.*, **49**, 736-768.

Vedder, W. & McDonald, R.S. (1963): Vibrations of OH^- ions in muscovite. *J. Chem. Phys.*, **38**, 1583-1590.

Wilkins, R.W.T. & Ito, J. (1967): Infrared spectra of some synthetic talcs. *Am. Mineral.*, **52**, 1648-1661.

Received 21 August 2000
Modified version received 18 December 2000
Accepted 6 February 2001